AIAA 2004-

High Energy Boundary Conditions for a Cartesian Mesh Euler Solver

Shishir A. Pandya
NASA Ames Research Center, Moffett Field, CA

Scott M. Murman
ELORET, Moffett Field, CA

Michael J. Aftosmis
NASA Ames Research Center, Moffett Field, CA

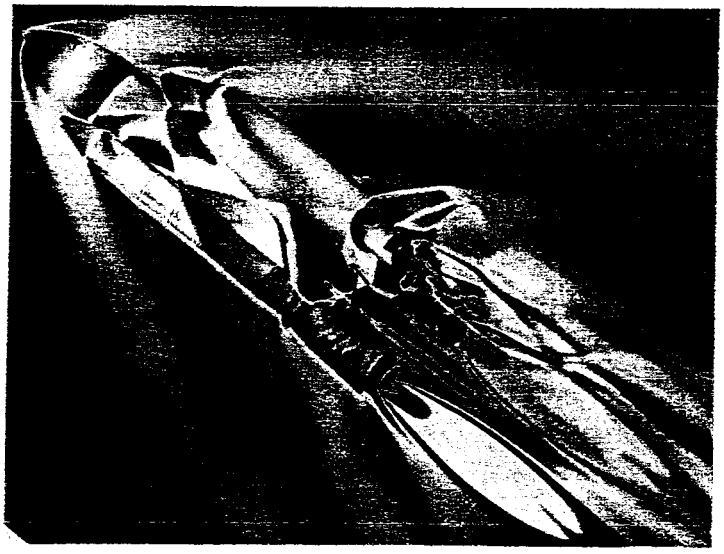

22nd AIAA Applied Aerodynamics Conference and Exhibit
16-19 August 2004 / Providence, RI

High Energy Boundary Conditions for a Cartesian Mesh Euler Solver

Shishir A. Pandya *
NASA Ames Research Center, Moffett Field, CA

Scott M. Murman †
ELORET, Moffett Field, CA

Michael J. Aftosmis ‡
NASA Ames Research Center, Moffett Field, CA

Abstract

Inlets and exhaust nozzles are often omitted or fared over in aerodynamic simulations of aircraft due to the complexities involved in the modeling of engine details such as complex gometry and flow physics. However, the assumption is often improper as inlet or plume flows have a substantial effect on vehicle aerodynamics. A tool for specifying inlet and exhaust plume conditions through the use of high-energy boundary conditions in an established inviscid flow solver is presented. The effects of the plume on the flow fields near the inlet and plume are discussed.

Introduction

Inlets and exhaust nozzles are common place in the world of flight. However, for the purposes of aerodynamic simulation, inlets and exhausts are often fared over and it is assumed that the flow differences resulting from this approximation are minimal. While this is an adequate assumption in many cases, the presence of an inlet that draws flow in or an exhaust with a substantial plume can have a notable effect on the flow field and thus the forces and moments of the vehicle. One such example is a jet-plume-induced flow separation on the surface of the vehicle [1]. The flow field in and near the base region is often mis-predicted resulting in incorrect base drag. For example, today's missiles have engines which produce an under-expanded plume which creates a blockage to the main flow. This blockage is unaccounted for without the modeling of the plume and can be important in obtaining accurate forces and moments. Thus, there is a need for proper modeling of high energy boundaries in the flow field. The lack of a plume can also create an evacuated base region thus effecting both drag and pitching moment values.

Often the lack of proper modeling of the inlet and exhaust conditions is due to the complexity of having to model a turbine engine. Often it is the details of the chemical processes in the combustion that keep engineers from modeling a plume. Thus, an engineering approximation that captures the aerodynamic effects of an inlet or exhaust on the vehicle without the complexity of modeling an engine's internal processes is needed. To remedy this, inlet and exhaust capability is added to an existing aerodynamic simulation package with the goal of accurately modeling these effects on vehicle aerodynamics. This goal is achieved by employing a high-energy boundary condition at a compressor face within an inlet duct and at a planar face within the nozzle.

The capability is added to the Cartesian mesh based aerodynamic simulation package CART3D[2]. The CART3D package consists of

*Aerospace Engineer, Member AIAA
†Senior Research Scientist, Member AIAA
‡Aerospace Engineer, Member AIAA

a set of tools for automatically and efficiently generating a Cartesian volume mesh from component triangulations. The flow solver within the CART3D package is an efficient, parallel, inviscid solver for a Cartesian mesh[3, 4].

The method for specifying the high-energy boundary conditions consists of a components based approach where each triangle is assigned a component number. These component numbers are assigned a boundary condition and a reference state in the flow solver. The flow solver is modified to use this information to produce the appropriate inlet or exhaust behavior at the given boundary using a characteristics based approach. A method for marking the inlet or exhaust plane triangles as separate components and the modifications to the flow solver are discussed.

The use of the present tool is demonstrated with validation test cases. A pitot type inlet and a wedge-shaped diffuser for which the conditions are predictable based on the normal and oblique shock relations show the capability of the method for inlet cases. The solution of the flow about an ogive shaped missile body is compared to an experiment[5] to demonstrate the exhaust capabilities of the tool. A space shuttle in ascent configuration is also computed to further show the usefulness of the tool in real world scenarios.

Method

A Riemann based boundary condition where the user can specify the known state at the boundary is used. A high energy state can be specified by the user at the boundary. The solution of the Riemann problem subsequently determines the conditions in the cells next to the boundary resulting in either inlet or exhaust.

Two tasks need to be accomplished in order to implement such a boundary condition. First, the set of triangles making up an inlet or an exhaust nozzle need to be marked appropriately so that the flow solver can easily distinguish them from other triangles. Second, the flow solver must treat these triangles in an manner appropriate to the conditions specified by the user.

Marking the triangulation

CART3D relies on a component wise approach to compose triangulated surfaces. In this approach, each component of the geometry is separately triangulated. All triangulated parts are then combined by intersecting the component triangulations. At the end of the intersection process, a single, closed, triangulated surface is obtained on which each triangle's origin can be identified by its component number.

A simple and effective strategy for identifying an inlet plane or an exhaust nozzle in this context is to assign a separate component number to the triangles that belong to an inlet or exhaust plane. However, inlet and/or exhaust planes are usually not modeled as separate components during the CAD process and often the geometry is an old triangulation that does not have its components identified. For these cases, a tool to extract the inlet and exhaust planes as components is used.

Presently, the tool allows the user to specify either a bounding box(a rectangular cube) or a sphere to mark an inlet or exhaust region. Any triangle within these regions is marked by the tool according to the user specification.

Figure 1(a) shows a legacy geometry where at the back end of a shuttle orbiter the exhaust planes for the 3 Space Shuttle Main Engine nozzles need to be extracted as separate components. The user specifies a sphere as shown in Fig. 1(b) to extract the exhaust plane of the top nozzle as a separate component. Figure 2 shows the resulting component marking. Each component is shown in a distinct color.

Flow solver algorithm

The boundary in the CART3D package is described by the surface triangulation. When the Cartesian mesh is generated, a set of cut cells is computed by intersecting the triangulation with the Cartesian cells forming a set of cut cells around the surface of the geometry. These cut cells are arbitrary polygons in 2D and polyhedra in 3D.

At an inlet or an exhaust plane, the user specified reference state is the flow condition at the boundary. As shown in Fig. 3 the flow condition at the boundary is denoted U_L. The flow condition in the cut-cell next to the boundary is reconstructed from the flow variables in the local neighborhood and is denoted U_R. A Riemann problem is then solved to compute the flux across that piece of the cut cell.

The result is that for supersonic flow the boundary reference state specified by the user becomes

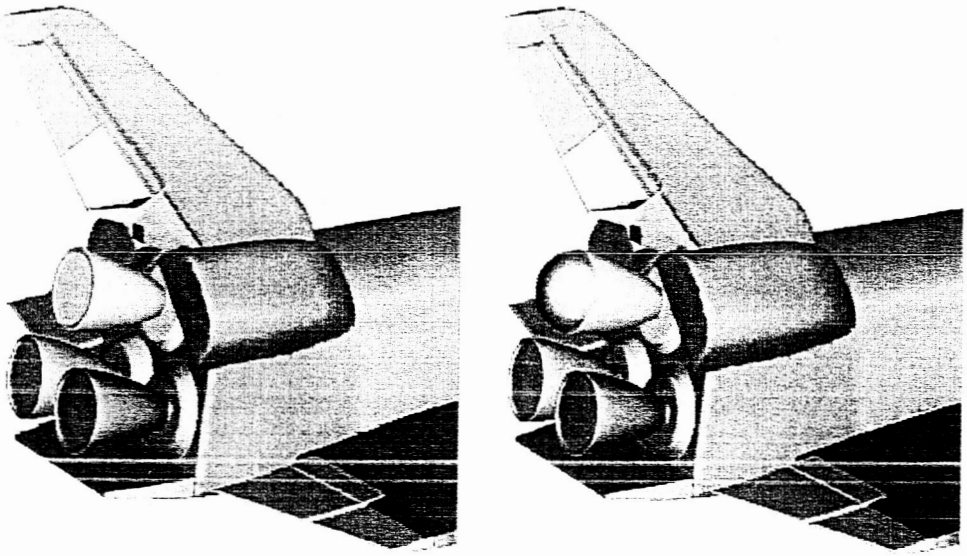

Fig. 1 Marking the triangles as inlet or Exit

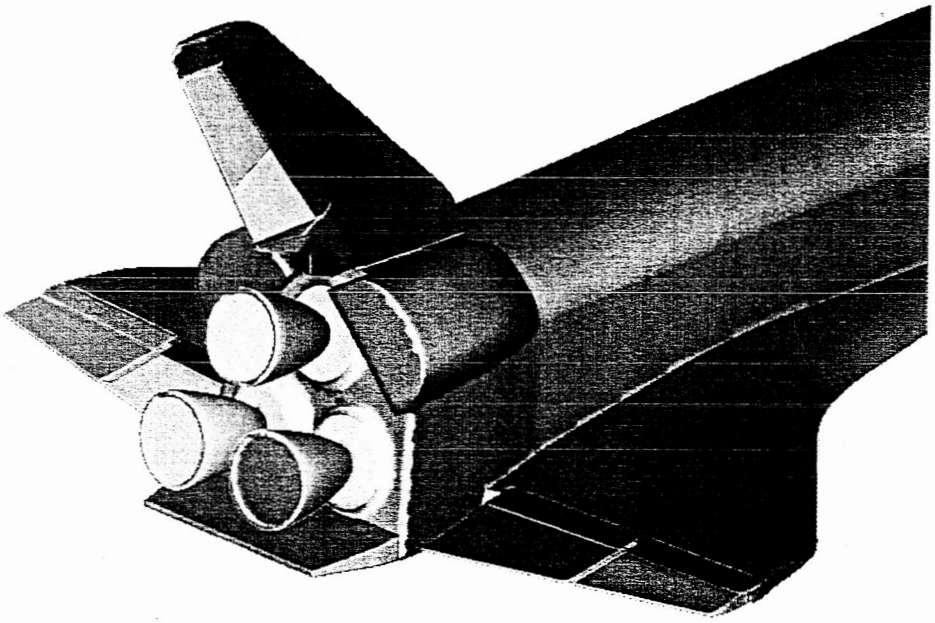

Fig. 2 Marking the triangles as inlet or Exit

the state at an exhaust plane. At a supersonic inlet, the result of the Riemann solver is to simply suck in whatever fluid is seen by the inlet plane. For subsonic flow, the Riemann solver computes an appropriate boundary value based on the characteristics of the flow and the specified boundary state.

An additional complication is that when the Riemann problem is solved in a non Cartesian-aligned plane, the velocity sent to the Riemann solver must be rotated into the coordinate system aligned with the normal to that boundary face. Once the Riemann problem is solved, the resulting flux must be rotated back to the original frame of reference and then added to the appropriate flux.

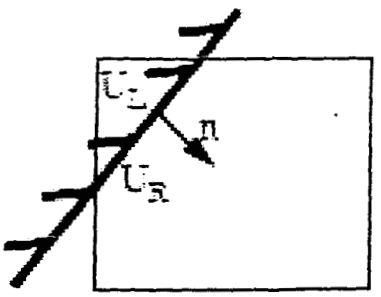

Fig. 3 A typical cut cell. The Cartesian cell is cut by a boundary forming a cut cell.

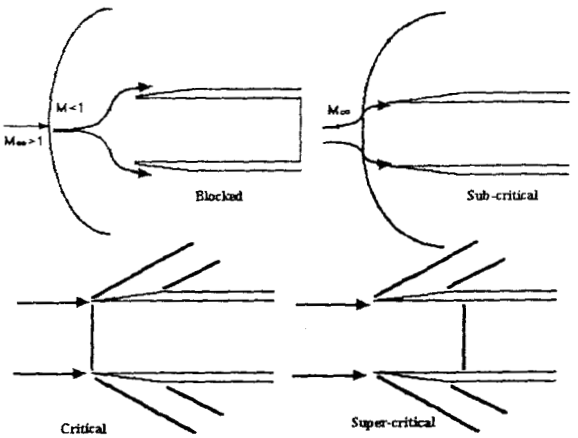

Fig. 4 The pitot intake

Results

Supersonic intake design depends heavily on the shock-systems that develop in the flow field. For this reason, two supersonic intakes are used to validate the method. A pitot intake is used to show that the method is capable of predicting the correct shock behavior. For a more complex shock system, a Wedge shaped diffuser where an oblique shock off the lip of the wedge slows the flow initially and a strong shock at the lip of the cowell reduces the flow speed to subsonic.

Following the inlet results, two exhaust validation test cases are presented followed by a Space Shuttle in the ascent configuration. An ogive shaped missile body at $M = 0.9$ for which the plume effects the pressure on the rear part of the body is simulated for several plume shapes. The plume size is controlled by the pressure in the plenum chamber. The results are compared to an experiment by Burt[5]. Finally, the full space shuttle stack with all the details of attachment hardware etc. is modelled with the plume on to demonstrate the ultimate usefulness of the method.

Pitot intake

The pitot intake can often be attractive to a designer due to its low drag. It is also an attractive test case for validation as its behavior is predictable. The behavior of the pitot intake is depicted in fig. 4 for four cases. In case one, the intake is blocked. The flow can not go though the intake. This results in a bow shock well ahead of the intake. In case two, there is flow through the intake, there is still some spillage resulting in a bow shock closer to the intake lip. This case is termed sub-critical. The third case, termed critical, does not let flow spill around the lip. This results in a normal shock at the lip. This condition is also called the maximum flow condition. In the fourth case, the pressure in the channel is lower than the critical case resulting in a delayed shock. Thus, the shock occurs well inside the intake channel.

The computation of these cases is performed on a Cartesian mesh which was refined in and near the intake channel to capture the shocks properly. The free stream Mach number for all four cases is 1.4. The critical condition for the test case is derived based on the normal shock relations as follows. For Mach number of 1.4, we obtain a Mach number in the channel of 0.7397 from the normal shock relations. The same relations also provide the pressure and density ratios as 2.1199 and 1.6896 respectively.

Figure 5(a) shows pressure contours from a computation of the case where the intake is not letting flow through. It can be seen that a bow shock well ahead of the intake lip has formed as expected. and the flow behind the bow shock is subsonic as expected. Four particle traces are released to verify that the flow is indeed going around the lip. The conditions at the intake tube wall are specified to be zero velocity for the blocked intake case.

The pressure contours for the sub-critical case are shown in fig. 5(b). Here a bow shock is seen just ahead of the intake lip. The particle traces verify that air is flowing through the intake, but some air spills to the outside. A higher than critical pressure is used to specify the boundary conditions for the sub-critical case.

The pressure contours for the critical case are shown in fig. 5(c). Here a normal shock forms at

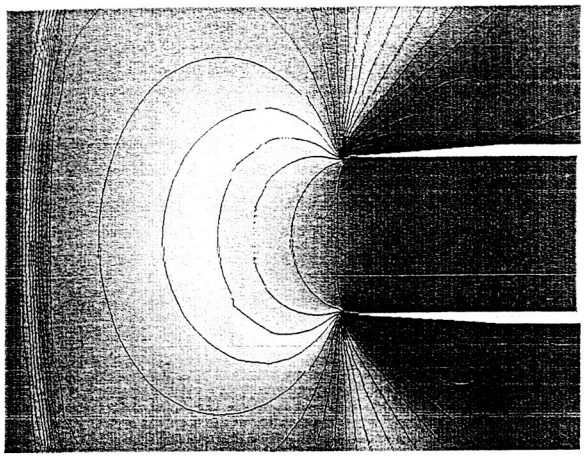

a) blocked

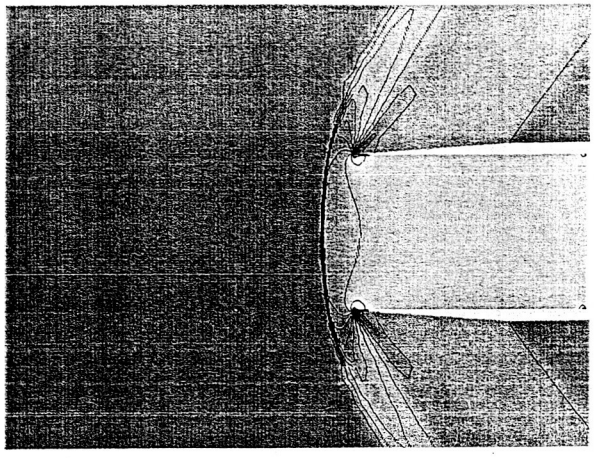

b) sub-critical

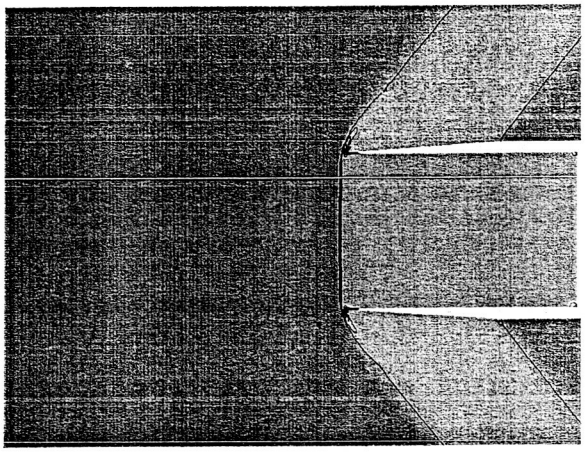

c) critical

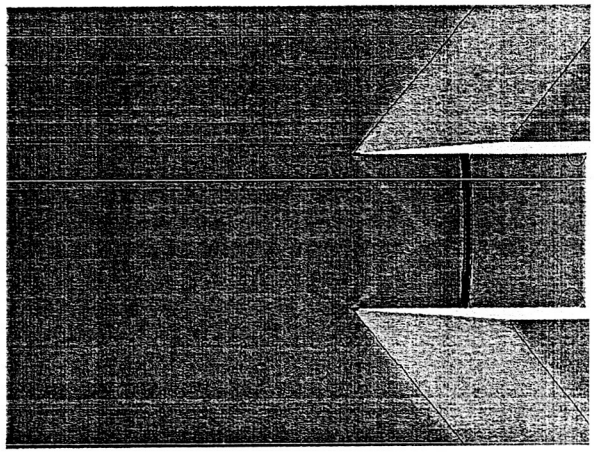

d) super-critical

Fig. 5 The pitot intake at $M_\infty = 1.4$

the intake lip as expected. To verify that the maximum flow condition has been achieved, particle traces are shown. The particle traces verify that no air from the area directly in front of the intake spills to the outside. The critical conditions discussed above are specified for this test case.

The pressure contours for the super-critical case are shown in fig. 5(d). Here the normal shock is seen inside the intake channel. The particle traces verify that no air spills to the outside of the lip. A lower than critical pressure is used to create the super-critical conditions.

Two-shock wedge diffuser

The normal shock diffuser is depicted in fig. 6. A 5° wedge shaped inlet results in an oblique shock followed by a normal shock at the cowell lip. The weak shock solution can be found from the oblique shock tables[6] for a free stream speed of $M_\infty = 2.0$. The pressure and density ratios

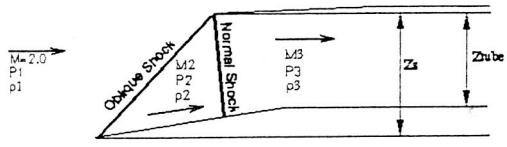

Fig. 6 The two shock Wedge diffuser

across the shock as well as the speed of the flow behind the shock are obtained using the oblique shock relations. When a second so called normal-shock occurs at the lip of the inlet, the condition is deemed to be the maximum flow condition as the flow through the inlet duct for this case corresponds to the maximum possible flow in the capture area(Z_s). The second shock is in reality is a strong shock solution of the oblique shock relations for a turn angle of 5° which corresponds to a shock angle of 86.36°. The flow behind the

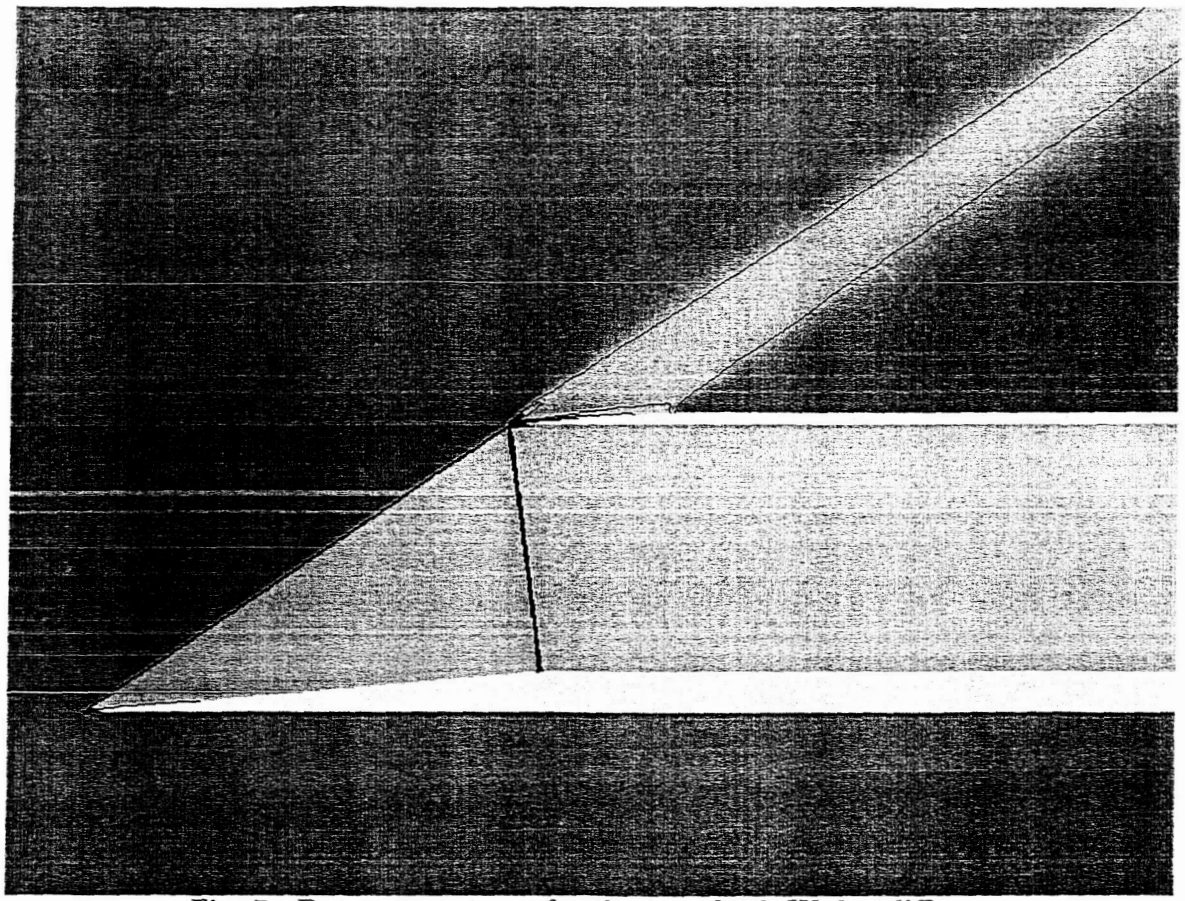

Fig. 7 Pressure contours for the two shock Wedge diffuser

shock is subsonic.

Based on the maximum flow condition, the area of the inlet is computed using the conservation relation,

$$\rho_1 u_1 Z_s = \rho_3 u_3 Z_{tube} \qquad (1)$$

A geometry of the wedge and inlet duct that corresponds to this area is created and the reference condition computed based on the oblique shock relations is specified at the inlet face. The results of the simulation are plotted as contours of the Mach number in figure 7. The expected solution corresponding to the maximum flow condition has been obtained with the appropriate shock angles and speeds.

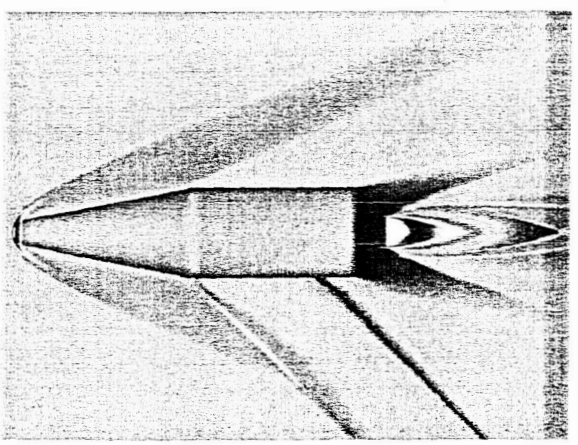

Fig. 8 Density contours on the surface of the FESTIP and the center plane at $M_\infty = 2.98$ compared to Experiments[7]

FESTIP

In addition to the being able to predict the inlet flows correctly, the method is also capable of accurately predicting the effects of an exhaust plume. We first focus our attention on the general features of the flow field with the plume on. In order to verify that we obtain a properly sized plume and that we are able to capture the effects of the plume on the flow field, the Future. European Space Transportation Investigation Program(FESTIP) at Mach 2.98 is simulated with plume conditions specified [7]. The resulting flow field is shown in fig. 8 and will be compared to a Schlieren photograph to show that the plume shape, size and its effects on the flow field are properly captured.

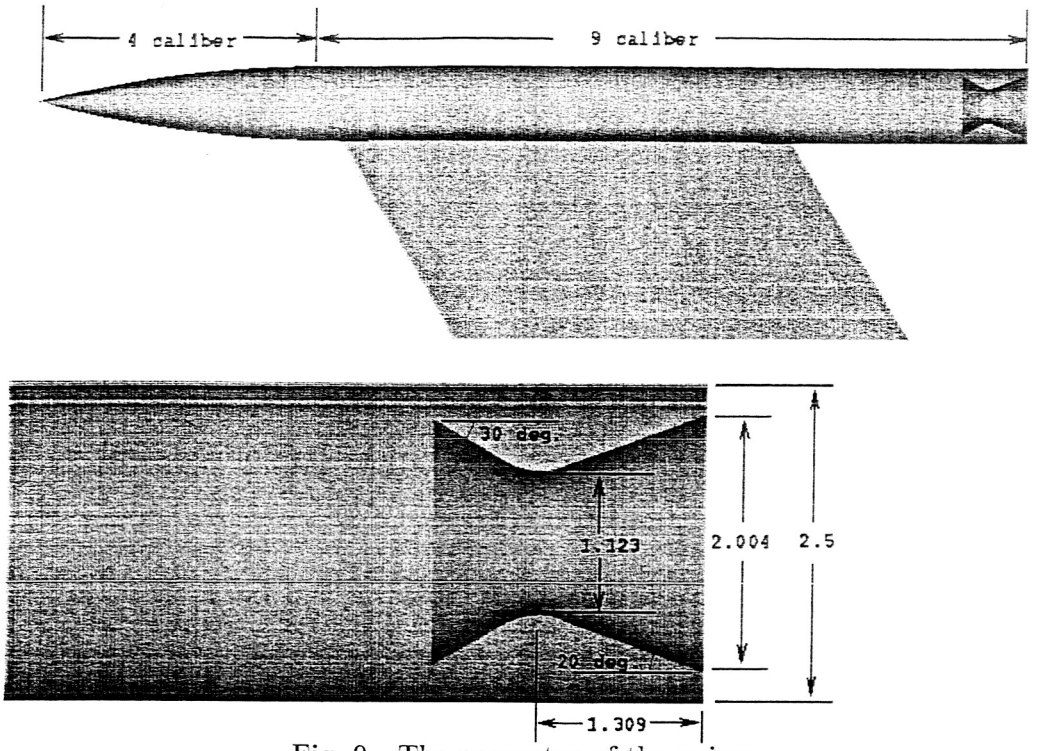

Fig. 9 The geometry of the ogive

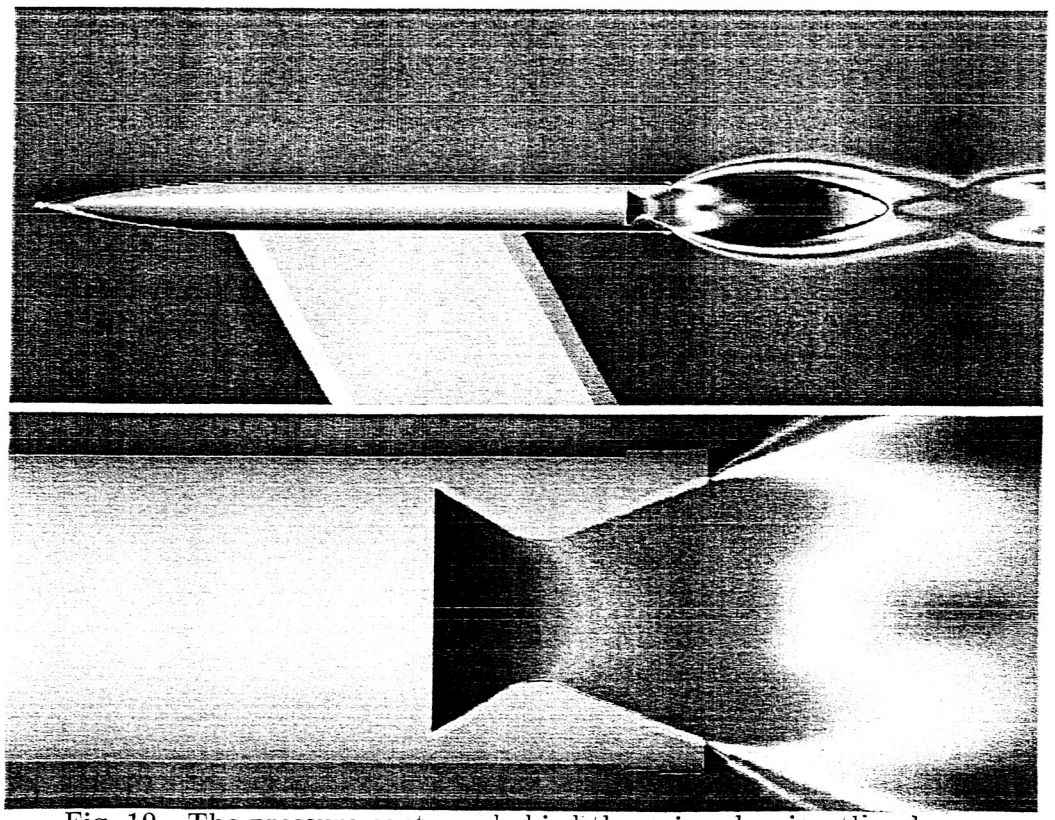

Fig. 10 The pressure contours behind the ogive showing the plume

Ogive

To further validate the plume capability of the high-energy boundary conditions, we look at a case for which the effect of the plume on the surface of the body is experimentally documented for several plume conditions. As the pressure in the plenum chamber is increased, a larger plume results and subsequently effects the pressure on the cyndrically shaped back part of the missile shaped ogive body. These changes in pressure effect the moments on the vehicle and are thus important to capture accurately.

A strut mounted body of revolution (see Fig. 9) with a cylindrical after-body is used in an experiment by Burt [5] at $M = 0.9$ and $M = 1.2$ with zero angle of attack. This case has been more recently computed by Raghunathan et. al [8] using a viscous technique. The model has a 4-caliber tangent ogive nose attached to a 9-caliber cylindrical body. A 20 deg conical nozzle with a design Mach umber of 2.7 is modeled to match the experiment.

Conditions are specified at the vertical face in the plenum chamber which correspond to the experimental conditions including the Pressure ratio between the plenum and the free stream. The specification of the pressure in the plenum provides the mechanism by which the air is pushed through the throat and the nozzle. The resulting plume is depicted by Mach number contours in Fig. 10 where blue denotes a slow speed flow such as that in the plenum, white denotes the high speed flow at approximately Mach 7 and the colors in between denote intermediate values.

The pressure on the surface of the cylindrical after-body is reported by the experiment [5]. The lowest pressure ratios correspond to an over-expanded plume while high pressure ratios correspond to an under-expanded plume. A blockage to the main flow develops as a result of the under-expanded plume. The plume grows larger with higher pressure ratios. Thus, at high pressure ratios the plume has a larger effect on the aerodynamics in the region of the cylindrical after-body. This effect can be seen by examining the changes in pressure on the after-body. The pressure on the after-body is therefore compared to the experiment and shows good agreement in both trend and value.

A similar plot on the same body for Mach number 1.2 is also shown in figure 12. For this supersonic speed case, the vehicle develops a shock on the cylindrical after-body due to the blockage from the under-expanded plume. Due to the boundary layer development, the compression in the experiment is not as strong as the inviscid simulation and as is well-known, the shock location is not well-predicted by the solution of the Euler equations.

In the experiment by Burt, a strut is used to mount the model in the wind tunnel [5]. The presence of the strut also has an effect on the flow field of the cylindrical after-body. This effect is investigated in the present work and shows that the pressure on the cylindrical after-body rises earlier. A small bump in pressure is visible due to this early rise as compared tot eh case without

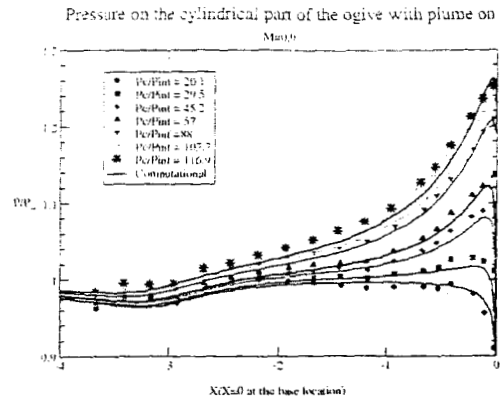

Fig. 11 Pressure on the surface of the ogive at $M_\infty = 0.9$ compared to Experiments[5] (x=0 is the base of the ogive body)

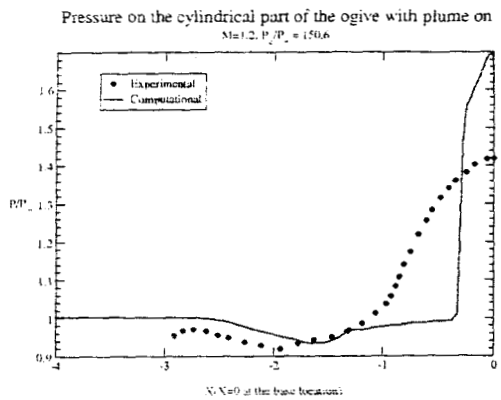

Fig. 12 Pressure on the surface of the ogive at $M_\infty = 1.2$ compared to Experiments[5] (x=0 is the base of the ogive body)

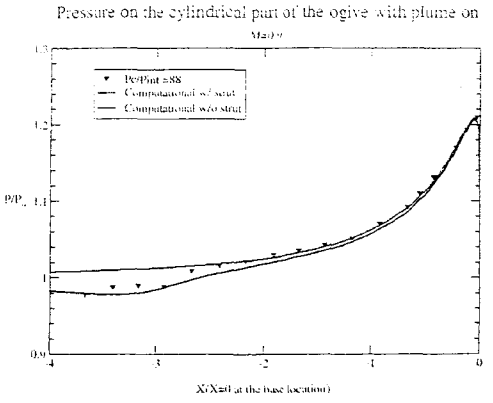

Fig. 13 Pressure rise on the cylindrical after-body of the ogive at $M_\infty = 0.9$ with and without the strut (Pressure ratio=88)

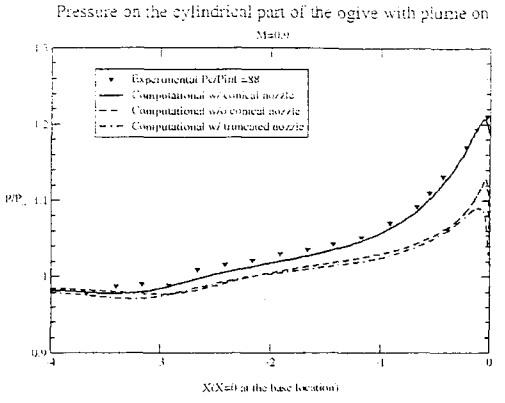

Fig. 14 Difference in pressure on the cylindrical after-body of the ogive at $M_\infty = 0.9$ with and without conical nozzle (Pressure ratio=88)

the strut as shown in fig. 13 for a pressure ratio of 88.0.

The present tool makes it possible for a user to specify the boundary conditions at one of several locations. One approach may be to specify the conditions at the exit plane. The advantage of this approach is that the details of a nozzle duct do not need to be modeled making the geometry much simpler. However, in the course of the implementation of this tool it is observed that the geometry of the nozzle is an important aspect of the flow modeling as the flow leaving the exit plane can not be assumed to be a constant profile across the plane. To illustrate this point, fig. 14 shows the comparison between the pressure on the after-body with and without the modeling of the nozzle. Also shown is the modeling when only a part of the nozzle (from throat to exit plane) is modeled. When the nozzle is not modeled or partially modeled, isentropic flow relations are used to obtain the conditions at the throat and subsequently at the exit plane. It can be concluded that the modeling of the nozzle geometry is essential to accurately predicting the pressure on the surface of the vehicle.

Space shuttle

The Space Shuttle simulation is performed to show the ultimate usefulness of the capability. Similar simulations have been performed in the past using structured overset meshes [9, 10]. Like the overset method, the Cartesian method offers complex geometry capability. The CART3D code makes it possible to generate meshes on highly complex configurations such as the space shuttle in ascent configuration in a very short time. This capability is combined with the high-energy boundary conditions to obtain a solution of the aerodynamics on the shuttle with the plume on. Figure 15 shows the Mach number contours on the surface of the Space shuttle as well as in selected cutting planes in the vicinity of the plumes. Though all three Space shuttle main engines(SSME) are active, only two are shown to be active in order to keep the third engine from blocking the view of the plumes.

Concluding remarks

A high-energy boundary condition is implemented in a Cartesian method to model inlet flows and exhaust plumes on aircraft, spacecraft and missiles. Their proper modeling and the resulting effect on vehicle aerodynamics is needed to accurately predict the forces and moments on the vehicle.

Two supersonic inlet designs that have subsonic flow in the inlet duct are used to validate the method for inlet flows. A pitot inlet and a two-shock wedge shaped inlet show that the method accurately predicts the location and stregth of the shocks. Two exhaust plume cases are compared to experiment to validate the exhaust capability of the method. The first case shows that the size and shape of the plume as well as its effect on the flow field are well predicted. The second test case is a numerical comparison of the pressures on the after-body as a function of a changing plume. It is comcluded that the modelling of the nozzle

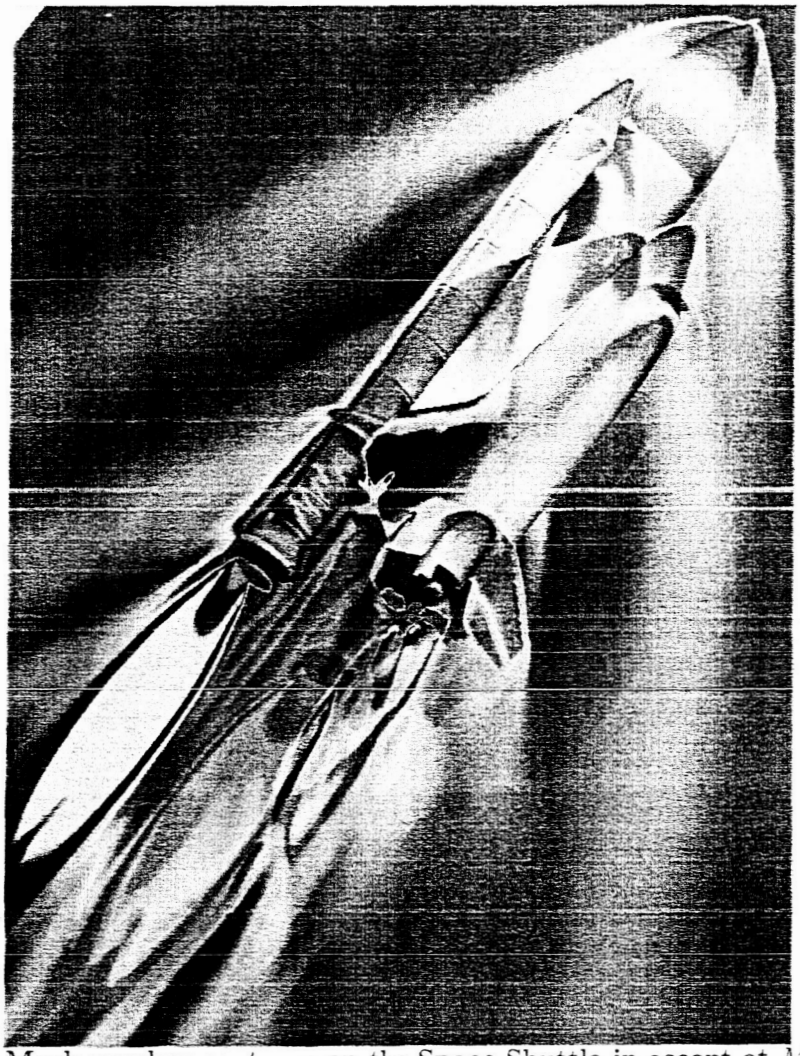

Fig. 15 Mach number contours on the Space Shuttle in ascent at $M_\infty = 2.46$

internal geometry is necessary in order to accurately predict the plume. The effects of the strut on which the wind tunnel model is mounted is also shown.

The high-energy boundary condition is a simple method for a non-expert user to specify inlets and exhausts.

Acknowledgment

The authors wish to thank Mike Olsen and William Chan of NASA Ames for his invaluable input during the course of this work.

References

[1] Robert J. McGhee. Jet-induced flow separation on a lifting entry body at mach number from 4.00 to 6.00. NASA Technical Memorandum NASA TM X-1997, NASA Langley Research Center, April 1970.

[2] M. J. Aftosmis, M. J. Berger, and J. E. Melton. Robust and efficient cartesian mesh generation for component-based geometry. AIAA Paper 97-0196, January 1997.

[3] M. J. Aftosmis, M. J. Berger, and G. Adomovicius. A parallel multilevel method for adaptively refined cartesian grids with embedded boundaries. AIAA Paper 2000-0808, January 2000.

[4] M. J. Aftosmis, M. J. Berger, and G. Adomovicius. Parallel multigrid on cartesian meshes with complex geometry. In *Proc. of the 8th Intl. Conf. on Parallel CFD*, Trondhiem Norway, June 2000.

[5] James Robert Burt. An investigation of the effectiveness of several devices in simulating a rocket plume at free stream mach numbers of 0.9 to 1.2. Technical Report RD-TR-71-22, U. S. Army Missile Command, Redstone Arsenal, Alabama, September 1971.

[6] Ames Research Staff. Equations, tables, and charts for compressible flow. Technical re-

port, Ames Aeronautical Laboratory, Moffett Field, CA, 1953.

[7] W. J. Bannink, E. M. Houtman, and P. G. Bakker. Base flow / underexpanded exhaust plume interaction in a supersonic external flow. AIAA paper 98-1598, 1998.

[8] S. Raghunathan, H. D. Kim, E. Benard, P. Malon, and R. Harrison. Plume interference effects on missile bodies. *J. Spacecraft*, 40(1):136–138, 2002.

[9] J. P. Slotnick, M. Kandula, and P. G. Buning. Navier-stokes simulation of the space shuttle launch vehicle flight transonic flowfield using a large scale chimera grid system. AIAA paper 94-1860, 1994.

[10] F. W. Jr. Martin, S. G. Labbe, T. C. Wey, and D. G. Pearce. Space shuttle launch vehicle wind tunnel and flight aerodynamic environments. AIAA paper 94-1861, 1994.